Precise control and displacement of polar textures from inhomogeneous and time-dependent electric fields

Fernando Gómez-Ortiz,* Louis Bastogne, Xu He, and Philippe Ghosez
Theoretical Materials Physics, Q-MAT, Université de Liège, B-4000 Sart-Tilman, Belgium

(Received 17 February 2025; accepted 2 April 2025; published 11 April 2025)

Since the discovery of polar topological textures, achieving their efficient control and manipulation has emerged as a significant challenge for their integration into nanoelectronic devices. In this study, we use second-principles molecular dynamic simulations to demonstrate the precise and reversible control of domain arrangements stabilizing diverse polarization textures through the application of various inhomogeneous and time-dependent electric fields. Furthermore, we conduct an in-depth study of ferroelectric domain motion under such fields, revealing features consistent with creep dynamics and establishing an upper limit for their propagation speed. Notably, our findings show that domain walls exhibit an asymmetric response delay, present at the onset of the dynamics but absent at its end. These findings provide valuable insights into the dynamical behavior of polar textures, which are relevant for the development of high-speed, low-power nanoelectronic applications.

DOI: 10.1103/PhysRevB.111.134107

I. INTRODUCTION

Inhomogeneous polar textures of ferroelectric materials have garnered substantial attention in recent years owing to their complex phase diagram [1], their nanometer length scales [2], their interesting functional properties such as negative capacitance [3] or chirality [4,5], and their ultrafast dynamics [6,7]. More recently, ferroelectric domain walls [8] and skyrmion bubbles [9] or, more generally speaking, ferroelectric bubble domains [10] have also emerged as promising nanoscale candidates for information carriers and with potential to revolutionize von Neumann computational approaches [11]. Due to their quasiparticle behavior [12] as well as their scalability [2], stability [9,13,14], stochastic dynamics [12,15,16], and controllable density [12,14,15,17], they are appealing for nanoelectronic applications such as racetrack memories [18] or token-based computing [11,19,20].

However, in order to exploit the potential of these inhomogeneous polar textures for practical applications, it is essential to develop precise methods for controlling both their instantaneous polarization state and their dynamical motion. Nucleation and growth of domains is a central topic of ferroelectrics and has been deeply studied [21–28]. Yet, the behavior of such domains under inhomogeneous and time-dependent electric fields, as well as the dynamics of complex polar textures, remains comparatively underexplored.

Lately, electric field pulses applied over mesoscopic regions [29–32] have been used to stimulate optical phonons in the material and stabilize different hidden phases by changing the frequency of the pulses or by recurrently applying them a concrete number of times. While promising, these methods have so far stabilized only specific phases, and deterministic control of the entire phase diagram for topological textures remains elusive. Additionally, predicting the resulting polar arrangement given the number of pulses, their duration, and the spacing between them is challenging. Recently, we proposed an alternative method showing the deterministic and dynamical tailoring of polar topologies using spatially modulated acoustic phonon excitations "APEX" [33]. Leveraging the strong coupling between polarization and strain in ferroelectric materials, the method uses acoustic phonons to generate strain fields that modulate the local polarization.

In this work, we demonstrate that the conceptual framework of inducing distortions with wave vectors $q \neq 0$ can be extended to spatially modulated electric fields, enabling comparable control and manipulation of polar textures. Furthermore, we perform an in-depth study of the dynamics of ferroelectric domain walls under inhomogeneous and time-dependent electric fields, revealing features consistent with the creep dynamics [26,27], unveiling the response delay of ferroelectric domain walls, and focusing on the mechanisms governing their motion and the critical velocities they can reach, which exceed those observed in their magnetic counterparts [34,35].

II. METHODS

Second-principles (SP) atomistic models were constructed using the MULTIBINIT [36] software by fitting data from density functional theory (DFT) calculations produced with the ABINIT [36] software package. The generalized gradient approximation (GGA) with the PBESol exchange-correlation functional and a plane-wave–pseudopotential approach with optimized norm-conserving pseudopotentials from the PseudoDojo server [37,38] were employed, considering as valence electrons $5d^{10}6s^26p^2$ for Pb, $3s^23p^63d^24s^2$ for Ti, and $2s^22p^4$ for O. A plane-wave energy cutoff of 65 Ha and an $8\times8\times8$ Γ-

*Contact author: fgomez@uliege.be

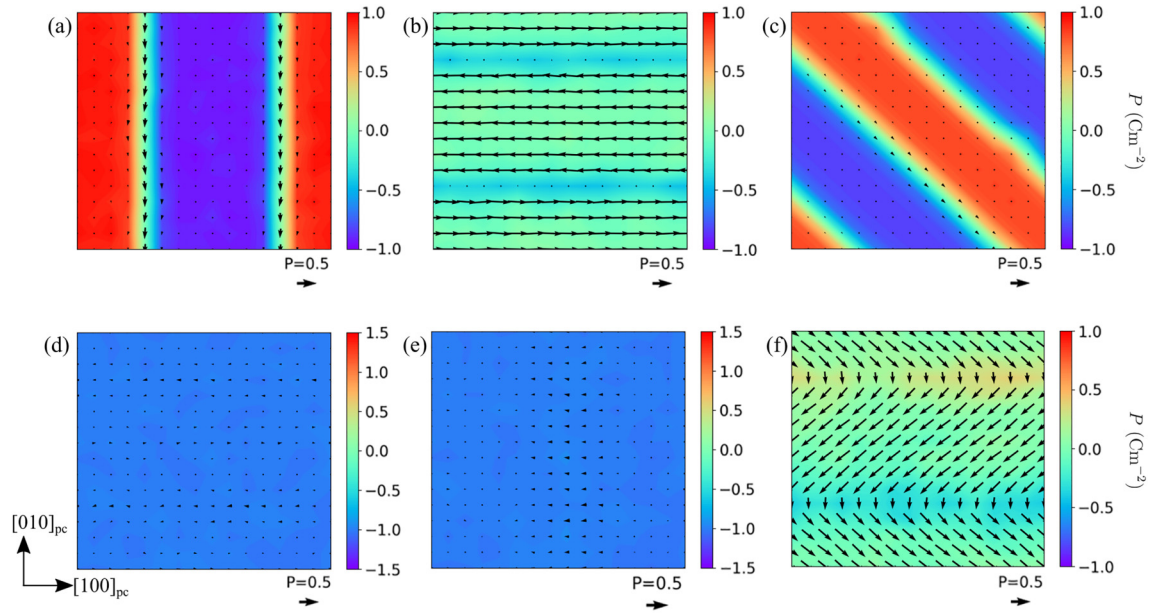

FIG. 1. Stabilization of different domain textures in bulk $PbTiO_3$ after the application of an inhomogeneous electric field with the functional form of Eq. (1). (a) $\lambda_x = 16$ u.c., $\mathbf{A} = 0.51(0, 0, 1)$ MV/cm. (b) $\lambda_y = 16$ u.c., $\mathbf{A} = 0.51(1, 0, 0)$ MV/cm. (c) $\lambda_x = \lambda_y = 16$ u.c., $\mathbf{A} = 0.51(0, 0, 1)$ MV/cm. (d) $\lambda_y = 8$ u.c., $\mathbf{A} = 1.54(0, 0, 1)$ MV/cm. (e) $\lambda_x = 16$ u.c., $\mathbf{A} = 25.7(1, 0, 0)$ MV/cm. (f) In-plane tensile strain $a = b = 3.955$ Å and $\lambda_y = 16$ u.c., $\mathbf{A} = 0.51(1, 0, 0)$ MV/cm. Arrows indicate the in-plane components of the polarization, whereas the color map represents the out-of-plane polarization. A reference arrow representing the scale of the in-plane polarization components is included.

centered k-point mesh were used. The harmonic part of the models was derived from density functional perturbation theory (DFPT) as implemented in ABINIT [36]. Dynamical matrices for the relaxed cubic $Pm\bar{3}m$ structure were computed using a $4 \times 4 \times 4$ q-point mesh. Various properties such as dipole-dipole interaction, Born effective charge, strain-phonon coupling, and elastic constants were extracted from the DFPT framework. The anharmonic part of the SP potential was fitted on a training set consisting of 3644 DFT configurations. A cutoff radius of $\sqrt{3}/2$ times the cubic lattice cell parameter was used to generate the anharmonic symmetry-adapted terms (SATs) from third to eighth order, considering strain-phonon coupling and anharmonic elastic constants. With this parameter set, 29 anharmonic SATs were automatically chosen to minimize energy forces and stresses through a goal function, and 66 additional terms were automatically produced to ensure the bounding of the SP potential. The model is described and available at Ref. [39].

Finite-temperature simulations were carried out using a hybrid molecular dynamics–Monte Carlo approach [40,41] to study the deterministic and dynamic switching of ferroelectric domains on a $16 \times 16 \times 4$ supercell. For the analysis of domain motion, regular molecular dynamics (MD) simulations in the canonical ensemble were employed on a $32 \times 32 \times 4$ supercell where four domains were explicitly included to eliminate potential spurious effects on the dynamics arising from periodic boundary conditions. A time step of 0.72 fs was used, ensuring accurate resolution of the dynamics relative to the periods of the applied electric fields.

In order to account for the effect of the inhomogeneous electric fields, an external force is added to each atom. Since the Born effective charge tensor $\mathbf{Z}^*$ describes the linear relationship between the force on an atom and the macroscopic electric field $\mathbf{E}$ [42], the force induced along β on an atom κ at a given position $\mathbf{r}$ by a field in direction α is equal to $F_{\kappa,\beta} = Z^*_{k,\alpha\beta} E_\alpha(\mathbf{r})$. We adopt the standard procedure where $\mathbf{Z}^*$ is computed in the reference cubic structure.

III. RESULTS

Let us first discuss the stabilization and dynamical control of different polar textures depending on the shape of the employed electric fields. We begin by focusing on simple domain structures that can be stabilized using a single modulated electric field before extending our analysis to more complex phases.

Stabilization of stripe domains. When the electric field has the functional form described by Eq. (1), where $\mathbf{A}$ dictates the amplitude of the electric field and $\boldsymbol{k}$ the modulation of the electric field in real space, stripe domains can be stabilized along different directions as shown in Fig. 1,

$$\mathbf{E}(\mathbf{r}) = \mathbf{A} \cdot \cos(\boldsymbol{k} \cdot \mathbf{r}) = \mathbf{A} \cdot \cos\left(\frac{2\pi x}{\lambda_x} + \frac{2\pi y}{\lambda_y} + \frac{2\pi z}{\lambda_z}\right). \tag{1}$$

The value of $\boldsymbol{k}$ will naturally determine the direction of the modulation of the domains and their periodicity in real space, whereas the value of $\mathbf{A}$ will determine the direction of the electric field. Therefore, if $\boldsymbol{k}$ and $\mathbf{A}$ are parallel (or antiparallel), the electric field will promote instable head-to-head and tail-to-tail domain walls, whereas if $\boldsymbol{k}$ and $\mathbf{A}$ are perpendicular, the electric field will couple with transversal optical modes and stabilize regular 180° domain walls in tetragonal ferroelectrics. Indeed, as shown in Figs. 1(a)–1(c), 180° domain walls can be observed in bulk $PbTiO_3$ where

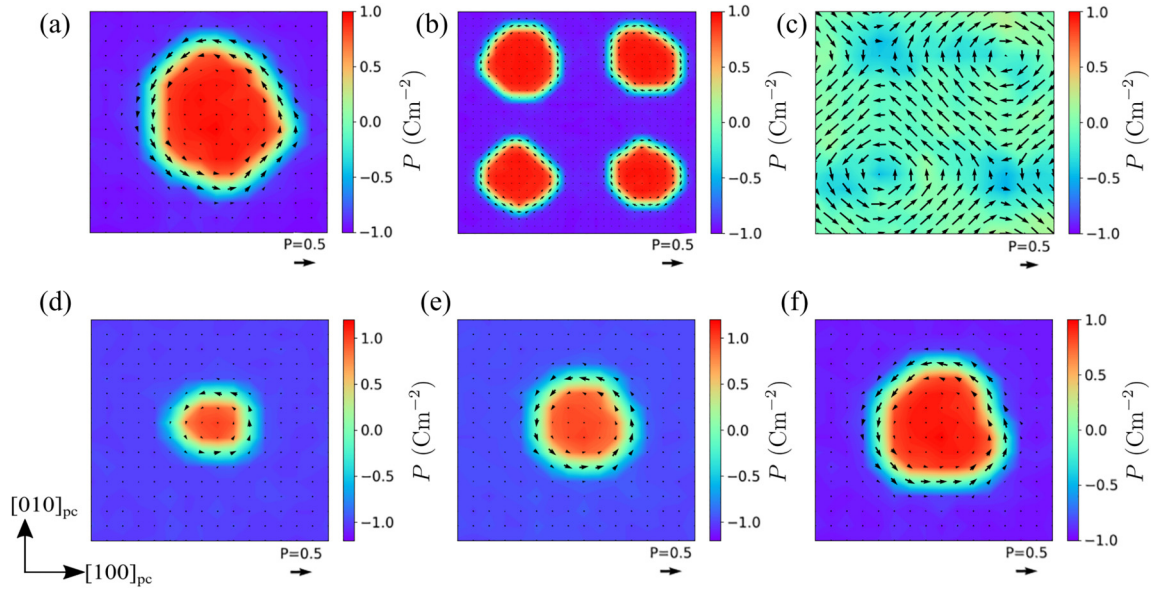

FIG. 2. Stabilization of different textures in bulk $PbTiO_3$ by means of different electric fields. (a),(b) Skyrmion lattice generated by the superposition of two cosine functions with periodicities of $\lambda_{1,x} = 16$ and $\lambda_{2,y} = 16$ u.c. and $\mathbf{A} = 0.51(0, 0, 1)$ MV/cm in a supercell of size $L =$ 16, 32 u.c., respectively. (c) Stabilization of a vortex/antivortex lattice in epitaxially strained $PbTiO_3$ $a = b = 3.955$ Å by the superposition of two cosine functions with periodicities of $\lambda_{1,x} = 16$, [$\lambda_{2,y} = 16$] u.c. and $\mathbf{A}_1 = 0.51(0, 1, 0)$, [$\mathbf{A}_2 = 0.51(1, 0, 0)$] MV/cm. (d)–(f) Individual skyrmion defects stabilized by the effect of Gaussian pulses as achievable by an AFM tip with different values of $\sigma = 4,\ 5,\ 6$ u.c., respectively. Arrows indicate the in-plane components of the polarization, whereas the color map represents the out-of-plane polarization. A reference arrow representing the scale of the in-plane polarization components is included.

Bloch-like polarization components emerge at the domain wall due to their ferroelectric character [43].

The polarization configuration obtained from our second-principles calculations does not necessarily mirror the applied electric field, as other relevant energy contributions are inherently at play. As a result, applying electric fields with very narrow periodicities or configurations that promote head-to-head or tail-to-tail domains will not necessarily produce such structures if they lead to energetically unfavorable or unphysical solutions for the system under study. For example, in bulk $PbTiO_3$, applying a periodicity of $\lambda = 8$ u.c. or smaller does not result in the formation of 180° domain walls with the imposed periodicity. Instead, the dipoles tilt towards the direction perpendicular to the modulation, forming a more uniform pattern that minimizes gradient energies, as shown in Fig. 1(d). Similarly, when an electric field favoring head-to-head and tail-to-tail domains is applied, these configurations are largely suppressed at low field magnitudes. As the field strength increases, a slight head-to-head or tail-to-tail configuration may emerge, but the system minimizes the electrostatic energy by lifting the dipoles towards the perpendicular direction to the modulation, thereby reducing the unfavorable bound charges arising from polarization divergence, as illustrated in Fig. 1(e). Even at high field magnitudes, the system strives to escape this energetically unfavorable situation. Likewise, if we apply sufficiently large tensile strain to $PbTiO_3$ ($a = b = 3.955$ Å, for instance) the regular 180° domains illustrated in Fig. 1(b) further evolve to textures with a nonuniaxial polarization pattern. Typically, they adopt a polarization wave arrangement as shown in Fig. 1(f). Interestingly, the PbO domain, which previously exhibited a ferroelectric instability along the z direction [see Fig. 1(b)], has now reoriented along the y direction while remaining perpendicular to the external applied field. This solution emerges in order to relax the elastic energy on the system.

Stabilization of more complex phases. More complex phases can also be stabilized with other electric fields or by the combination of several waves such as the ones used in the previous section. In particular, skyrmion textures can be stabilized in bulk $PbTiO_3$ [see Fig. 2(a)] by the superposition of two cosine functions with periodicities along x and y and electric field direction along z similar to the ones used in the previous section applied on top of a homogeneous background. Strictly speaking, this process promotes the formation of a square lattice of nanodomains with a periodicity corresponding to that of the initial wave that after relaxation, generates a square lattice of skyrmion bubbles as predicted in Ref. [44], as illustrated in Fig. 2(b). By doubling the simulation cell while maintaining the periodicity of the electric field modulation, a square lattice of similar size skyrmions is formed. It is noteworthy that the Bloch component of the domain walls (either clockwise or counterclockwise) varies between individual skyrmions stochastically, demonstrating that they are not identical periodic replicas of one another and granting different chiral nature to each of the defects. Upon increasing the tensile strain on the system ($a = b = 3.955$ Å), in-plane lattices of vortices and antivortices, as shown in Fig. 2(c), can be stabilized if two electric fields modulated along x and y and magnitudes along y and x, respectively, are applied on the system. The polarization wave previously stabilized under similar mechanical conditions showing a uniform polarization along the y direction [see Fig. 1(f)] is now unstable due to the effect of the second field modulated along x and with magnitude along y. As a consequence, closure

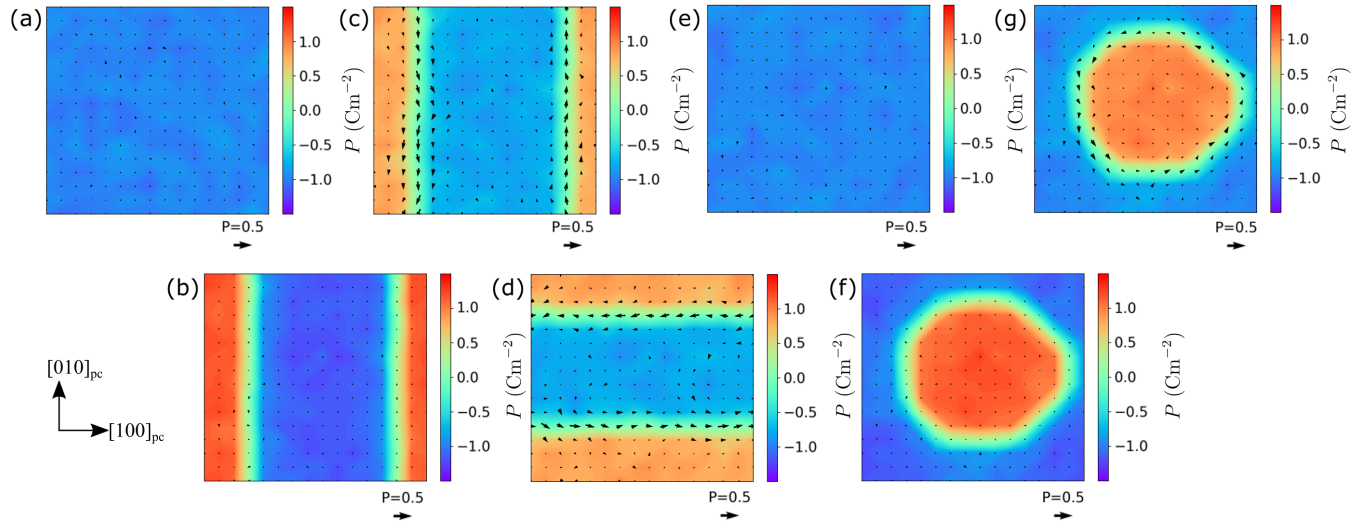

FIG. 3. Dynamical evolution of different textures in bulk $PbTiO_3$ stabilized by means of electric fields. (a) Initial phase showing a monodomain configuration. (b) Domain structure under the application of a modulated electric field following Eq. (1), $\lambda_x = 16$ u.c. and $\mathbf{A} = 5.14(0, 0, 1)$ MV/cm. (c) Relaxed domain structure after removing the electric field. (d) Relaxed opposite domain configuration after the application of a modulated field following Eq. (1), $\lambda_y = 16$ u.c. and $\mathbf{A} = 2.06(0, 0, 1)$ MV/cm. (e) Monodomain structure obtained under the application of a homogeneous field of magnitude 1.54 MV/cm. (f) Lattice of bubble domains after the application of two modulated fields along x and y with magnitude 5.14 MV/cm. (g) Skyrmion lattice after the relaxation of (f) under no external fields. Arrows indicate the in-plane components of the polarization, whereas the color map represents the out-of-plane polarization. A reference arrow representing the scale of the in-plane polarization components is included.

textures emerge in the system in order to comply with the imposed periodicity. This derives in the evolution of the previously uniform domain wall along the y direction, which now exhibits distinct internal domains, i.e., one with $P_y > 0$ (up) and the other with $P_y < 0$ (down). Therefore, under the conditions imposed by the modulated electric fields and the tensile strain, a transition from a uniform PbO ferroelectric domain wall [43] into an Ising line [45] occurs. Interestingly, these closure textures are stable even if they extend over large distances, allowing their nucleation with electric fields that do not require strong spatial modulation. The vortex/antivortex singularities are placed at the intersection between the two domain walls and centered on a Pb atom. Interestingly, we observe that an out-of-plane component of the polarization is prone to develop at those points, similarly to what happens in regular domain walls [43], which grants a nonzero topological character to these textures, effectively forming a meron/antimeron lattice. Similar in-plane vortex/antivortex textures, capable of extending over long distances without requiring highly spatially modulated fields, have already been predicted in $BaTiO_3$ and other rhombohedral ferroelectrics under comparable electric fields [46].

Single defects can also be stabilized by the effect of a Gaussian field when applied on a homogeneous background of opposite polarity mimicking the effect that can be achieved by an atomic force microscopy (AFM) tip in the laboratory, as anticipated in Ref. [44] or predicted in Ref. [15]. In a general formulation, such field can be written as

$$\vec{E}(\mathbf{r}) = \mathbf{A} \cdot e^{-(\boldsymbol{\mu}-\mathbf{r}-\mathbf{v}t)^2/\sigma^2}, \tag{2}$$

where $\boldsymbol{\mu}$ represents the center of the Gaussian field, σ its standard deviation, and $\mathbf{v}$ the velocity of the center of mass. By selecting different values of σ, different sizes of bubble domains can be stabilized, as can be observed in Figs. 2(d)–2(f). However, as discussed in the previous section, if lower values of σ are chosen, the applied field will be unable to nucleate any domain unless unrealistically large field amplitudes are employed. In such cases, the resulting domains will be unstable and collapse upon a monodomain phase after removing the bias.

Reversible and deterministic switching. One of the strengths of stabilizing different polar textures via applied electric fields, compared to conventional methods such as strain engineering [47] or varying growth conditions [48], is the ability to actively manipulate the polar state of the material, enabling real-time control. In the first part of the manuscript (Figs. 1 and 2), the initial structure before applying the electric field was the centrosymmetric cubic $Pm\bar{3}m$ phase for simplicity. However, as we will now discuss, similar control of the resulting phase are obtained when starting from an already polarized phase.

This section presents concrete examples in which domains along different directions or skyrmion lattices can be stabilized and dynamically switched between each other by varying the applied electric field to which they are subjected. To illustrate this, Fig. 3 collects the evolution of the system at the temperature of $T = 70$ K when different electric fields are applied.

Initially [Fig. 3(a)], we start with a monodomain structure obtained after poling the system with an homogeneous electric field. Then, we nucleate a domain structure periodically repeated along the x direction after the application of a field satisfying Eq. (1) with $\lambda_x = 16$ u.c. and $A_z = 5.14$ MV/cm [Fig. 3(b)] that relaxes upon removal of the electric field [Fig. 3(c)]. Such domain can be switched towards the y direction after the application of a softer field showing periodicity

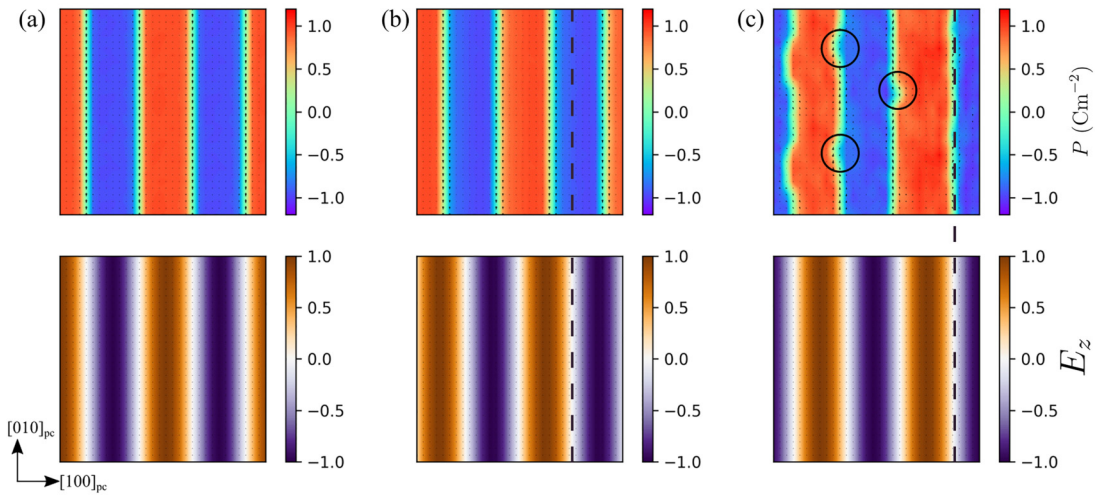

FIG. 4. Domain-wall motion in bulk $PbTiO_3$. Domain structure (upper row) and instantaneous electric field (bottom row) at (a) $t = 0$ s, (b) $t = 4.8$ ns, and (c) $t = 9.3$ ns. Arrows in the dipole patterns represent the in-plane components of the polarization. The color bar in the electric field represents its normalized value along the z direction. The dashed lines in (b) and (c) represent the location of the node of the electric field wave and the circles in (c) highlight domain nucleation points.

of $\lambda_y = 16$ u.c. and $A_z = 2.06$ MV/cm. Notably, these field-induced phases are long-lived metastable states and remain stable even after the field is removed [Fig. 3(d)]. This domain structure can be erased (by applying homogeneous electric fields $A_z = 1.54$ MV/cm) or rewritten back and forth at one's convenience following the previously described procedure. Moreover, we can transit between periodically repeated domain structures and lattices of the skyrmion if, instead of a single field modulated along x or y, we applied both fields at the same time, as shown in the previous section, $\lambda_{1,x} = \lambda_{2,y} = 16$ u.c. of magnitude $A_z = 5.14$ MV/cm [Fig. 3(f)]. After removing the field, the periodic lattice of bubble nanodomains further relaxes to a lattice of skyrmion textures demonstrating again the stability of the nucleated phases and their deterministic control, similar to that achieved via APEX [33].

Dynamics of ferroelectric domains. After stabilizing domain structures and demonstrating deterministic switching between different configurations, we now investigate how domain walls can be displaced using time-dependent electric fields. This section focuses on their mobility, examining how domain walls respond to changes in the electric field and how fast they can rearrange. In order to account for the time modulation of the electric field, an extra term needs to be added to the functional form presented in Eq. (1) that now reads

$$\mathbf{E}(\mathbf{r}, t) = \mathbf{A} \cdot \cos\left(\frac{2\pi x}{\lambda_x} + \frac{2\pi y}{\lambda_y} + \frac{2\pi z}{\lambda_z} + \frac{2\pi t}{T}\right), \quad (3)$$

where T is the period of the time modulation. The expected velocity of the electric field wave, corresponding to the propagation speed of its phase, is then given by $v = (1/\lambda_x^2 + 1/\lambda_y^2 + 1/\lambda_z^2)^{-1/2}/T$, which depends on the spatial and temporal periodicities and that in the most usual case of a single spatial modulation, reduces to $v = \lambda/T$.

The motion of domain walls is critical to many applications involving ferroelectric materials and has been deeply studied in the context of homogeneous electric fields under the nucleation and growth framework [23–27]. However, their behavior under inhomogeneous and time-dependent electric fields, as well as the dynamics of topological textures, remains comparatively underexplored except for few recent works [15,49].

In Fig. 4, we show the molecular dynamics results for the domain-wall motion under an external electric field of magnitude 2 MV/cm, periodicity $\lambda_x = 16$ u.c., and velocity $v = 300$ m/s. The temporal variation of the electric field imposes a constraint on the domain walls, requiring them to adapt to the periodic changes in the electric field. However, as revealed in Fig. 4(b), a noticeable lag in their response to the field's oscillations can be observed (see dashed line), proving a delay in the reaction time of the domains to the external driving force that amounts to 4 ps at $T = 5$ K for the 16 u.c. domain periodicity. Interestingly, this lag is only present at the onset of the dynamics; once the domains begin to move, the correlation between the domain-wall position and the node of the electric field wave becomes one to one [see dashed line in Fig. 4(c)]. Moreover, this lag shows a strong temperature dependence: when the system is heated to 100 K, the lag is reduced by half, and at 200 K, it already becomes negligible. Interestingly, when the electric field is removed, the domains stop moving immediately, showing no sign of residual momentum, although this observation can be slightly influenced as a consequence of the domain propagation mechanism.

Our MD simulations confirm that domain displacement follows the diffuse boundary model as proposed in Ref. [25]. As shown by the solid circles in Fig. 4, certain regions of the domain nucleate first, and the domain wall subsequently follows this initial nucleation, rather than propagating uniformly across the domain. Therefore, if the nucleus of the new domain exceeds a critical size, it can lead to the formation of an additional domain layer even after the electric field is removed. However, this phenomenon is more related to the relaxation of the domain structure than to an inertial response. While the absence of response delay upon field removal is consistent with the findings of Ref. [28], our results complement them by demonstrating a clear response delay at the

onset of domain-wall motion. This asymmetry in the response delay of domains comes from the intrinsic energy barrier for nucleation.

In addition, there are scenarios where domains remain immobile due to the high activation energy associated with their motion irrespective of the wave velocity. Our observations indicate, for instance, that domain mobility is strongly influenced by their size: domains with double periodicity (32 u.c.) remain static when the electric field is adjusted to match their modulation while retaining the magnitude that renders domains with a periodicity of 16 u.c. already mobile. The activation energy barrier can be mitigated by either increasing the temperature or enhancing the magnitude of the electric field applied to the domains. Specifically, when the periodicity of the domains and the corresponding electric fields is doubled, the field magnitude should also be doubled in order to produce sufficient force on the domains, enabling their movement. This relationship between activation energy, temperature, and electric field is consistent with the predictions of the creep law [26,27]. These adjustments enable domains to transition from an immobile to a mobile regime, allowing even larger domains to overcome their activation energy.

When the propagation speed of the electric field increases, the domain structure is unable to keep up with the rapid oscillations and eventually regions of negative electric field align with positive polarization regions. This misalignment induces a chaotic evolution in the system, leading to the fragmentation of the domain structure and marking the maximum velocity at which domains can move. In our case, with $\lambda_x = 16$ u.c. and a field amplitude of 2 MV/cm, this limiting velocity was approximately 3000 m/s, significantly higher than the 900 m/s recently reported for magnetic skyrmions [35]. If the wave velocity of the electric field is increased further, there is a threshold beyond which the domains become effectively immobile, no longer responding to the applied electric field. Interestingly, the limiting velocity at which domains lose connectivity and destabilize remains unaffected by changes in the electric field magnitude or temperature as long as the domains remain in the mobile regime. The domain structure consistently destabilizes at the same electric field velocity, marking an intrinsic upper bound on domain-wall motion that is probably related to the material and the stability of the multidomain structure.

Similar characteristics such as lag in response and asymmetric response delay, existence of a limiting velocity (which is indeed identical to the one previously reported), and diffuse boundary nucleation are also observed in the dynamics of bubble domains. In such a case, the motion of the bubble domains is governed by the elongation and contraction of their structure, resembling the deformation of a water droplet or the motion of an amoeba. Remarkably, the mobility of these bubble domains is isotropic, enabling them to move equivalently in any direction in response to the position of a Gaussian field, without exhibiting any preference for specific crystallographic directions. Furthermore, they can adapt to other waveforms, such as cosine functions, maintaining their structural integrity while being displaced by these periodic perturbations under appropriate electric field magnitudes.

IV. CONCLUSIONS

In this work, we first demonstrate the deterministic nucleation and precise control of various polar textures in the prototypical ferroelectric $PbTiO_3$ using spatially modulated electric fields.

Furthermore, we have investigated the motion of multidomain structures under inhomogeneous and time-dependent electric fields and observed a noticeable lag between the oscillations of the electric field and the response of the polar texture. This lag, which arises from the nucleation barrier of the polarization domains, is particularly evident at the onset of the dynamics and shows a strong temperature dependence, but becomes negligible once the domains achieve steady motion. Interestingly, such delay is not present when stopping the field, proving that domains show no residual momentum.

As the velocity of the electric field increases, the synchronization between the electric field and the domain structure is lost, ultimately leading to the fragmentation of the domain configuration. Notably, this limiting velocity is remarkably robust against variations in the electric field magnitude and temperature. However, it presumably depends on the material properties or the intrinsic stability of the domains. For instance, in ferroelectric/dielectric superlattices, where domains are inherently formed due to electrostatic conditions, the limiting velocity will likely be larger. Additionally, our simulations highlight the significant role of domain size in their mobility under inhomogeneous and time-dependent electric fields. Larger domains exhibit a higher activation energy barrier, rendering them immobile under conditions where smaller domains are already mobile.

These findings provide valuable insights into the intricate dynamics of domain walls and topological textures under inhomogeneous and time-dependent electric fields, shedding light on the fundamental mechanisms governing their motion. Moreover, in contrast to regular methods for the synthesis of topological textures that do not allow the modification of the polar arrangement once it is stabilized [47,48], our methodology allows one to dynamically manipulate polar textures *in situ*. While experimentally achieving spatially modulated electric fields at the nanometer scale remains challenging, recent advances in nanofabrication techniques [50] suggest that such fields may become feasible in the near future. We hope this work stimulates further development of these techniques, which would enable precise manipulation of topological polarization structures, offering new possibilities for next-generation nanoelectronic devices where fine control over ferroelectric phases is essential.

ACKNOWLEDGMENTS

F.G.-O. acknowledges financial support from MSCA-PF 101148906 funded by the European Union; the Fonds de la Recherche Scientifique (FNRS) through Grant No. FNRS-CR 1.B.227.25F; the Consortium des Équipements de Calcul Intensif (CÉCI), funded by the F.R.S.-FNRS under Grant No. 2.5020.11; and the Tier-1 Lucia supercomputer of the Walloon Region infrastructure funded by the Walloon Region under Grant Agreement No. 1910247. F.G.-O. and P.G. also

acknowledge support by the European Union's Horizon 2020 research and innovation program under Grant Agreement No. 964931 (TSAR). P.G. and X.H. also acknowledge support from the Fonds de la Recherche Scientifique (FNRS) through the PDR project PROMOSPAN (Grant No. T.0107.20).

DATA AVAILABILITY

The data that support the findings of this article are not publicly available. The data and the second-principles model are available from the authors upon reasonable request.

[1] J. Junquera, Y. Nahas, S. Prokhorenko, L. Bellaiche, J. Íñiguez, D. G. Schlom, L.-Q. Chen, S. Salahuddin, D. A. Muller, L. W. Martin, and R. Ramesh, Topological phases in polar oxide nanostructures, Rev. Mod. Phys. **95**, 025001 (2023).

[2] G. Catalan, J. Seidel, R. Ramesh, and J. F. Scott, Domain wall nanoelectronics, Rev. Mod. Phys. **84**, 119 (2012).

[3] J. Íñiguez, P. Zubko, I. Luk'yanchuk, and A. Cano, Ferroelectric negative capacitance, Nat. Rev. Mater. **4**, 243 (2019).

[4] L. Louis, I. Kornev, G. Geneste, B. Dkhil, and L. Bellaiche, Novel complex phenomena in ferroelectric nanocomposites, J. Phys.: Condens. Matter **24**, 402201 (2012).

[5] P. Shafer, P. García-Fernández, P. Aguado-Puente, A. R. Damodaran, A. K. Yadav, C. T. Nelson, S.-L. Hsu, J. C. Wojdeł, J. Íñiguez, L. W. Martin, E. Arenholz, J. Junquera, and R. Ramesh, Emergent chirality in the electric polarization texture of titanate superlattices, Proc. Natl. Acad. Sci. USA **115**, 915 (2018).

[6] D. Daranciang, M. J. Highland, H. Wen, S. M. Young, N. C. Brandt, H. Y. Hwang, M. Vattilana, M. Nicoul, F. Quirin, J. Goodfellow *et al.*, Ultrafast photovoltaic response in ferroelectric nanolayers, Phys. Rev. Lett. **108**, 087601 (2012).

[7] Q. Li, V. A. Stoica, M. Paściak, Y. Zhu, Y. Yuan, T. Yang, M. R. McCarter, S. Das, A. K. Yadav, S. Park, C. Dai, H. J. Lee, Y. Ahn, S. D. Marks, S. Yu, C. Kadlec, T. Sato, M. C. Hoffmann, M. Chollet, M. E. Kozina *et al.*, Subterahertz collective dynamics of polar vortices, Nature (London) **592**, 376 (2021).

[8] S. K. Streiffer, J. A. Eastman, D. D. Fong, C. Thompson, A. Munkholm, M. V. Ramana Murty, O. Auciello, G. R. Bai, and G. B. Stephenson, Observation of nanoscale 180° stripe domains in ferroelectric $PbTiO_3$ thin films, Phys. Rev. Lett. **89**, 067601 (2002).

[9] S. Das, Y. L. Tang, Z. Hong, M. A. P. Gonçalves, M. R. McCarter, C. Klewe, K. X. Nguyen, F. Gómez-Ortiz, P. Shafer, E. Arenholz, V. A. Stoica, S.-L. Hsu, B. Wang, C. Ophus, J. F. Liu, C. T. Nelson, S. Saremi, B. Prasad, A. B. Mei, D. G. Schlom *et al.*, Observation of room-temperature polar skyrmions, Nature (London) **568**, 368 (2019).

[10] Q. Zhang, L. Xie, G. Liu, S. Prokhorenko, Y. Nahas, X. Pan, L. Bellaiche, A. Gruverman, and N. Valanoor, Nanoscale bubble domains and topological transitions in ultrathin ferroelectric films, Adv. Mater. **29**, 1702375 (2017).

[11] D. Meier, J. Íñiguez-González, D. Rodrigues, and K. Everschor-Sitte, Editorial: Focus issue on topological solitons for neuromorphic systems, Neuromorph. Comput. Eng. **4**, 010202 (2024).

[12] H. Aramberri and J. Íñiguez-González, Brownian electric bubble quasiparticles, Phys. Rev. Lett. **132**, 136801 (2024).

[13] S. Das, Z. Hong, V. A. Stoica, M. A. P. Gonçalves, Y. T. Shao, E. Parsonnet, E. J. Marksz, S. Saremi, M. R. McCarter, A. Reynoso, C. J. Long, A. M. Hagerstrom, D. Meyers, V. Ravi, B. Prasad, H. Zhou, Z. Zhang, H. Wen, F. Gómez-Ortiz, P. García-Fernández *et al.*, Local negative permittivity and topological phase transition in polar skyrmions, Nat. Mater. **20**, 194 (2021).

[14] V. Govinden, S. Rijal, Q. Zhang, Y. Nahas, L. Bellaiche, N. Valanoor, and S. Prokhorenko, Stability of ferroelectric bubble domains, Phys. Rev. Mater. **7**, L011401 (2023).

[15] S. Prokhorenko, Y. Nahas, V. Govinden, Q. Zhang, N. Valanoor, and L. Bellaiche, Motion and teleportation of polar bubbles in low-dimensional ferroelectrics, Nat. Commun. **15**, 412 (2024).

[16] F. Gómez-Ortiz, M. Graf, J. Junquera, J. Íñiguez-González, and H. Aramberri, Liquid-crystal-like dynamic transition in ferroelectric-dielectric superlattices, Phys. Rev. Lett. **133**, 066801 (2024).

[17] Y. Nahas, S. Prokhorenko, Q. Zhang, V. Govinden, N. Valanoor, and L. Bellaiche, Topology and control of self-assembled domain patterns in low-dimensional ferroelectrics, Nat. Commun. **11**, 5779 (2020).

[18] S. S. P. Parkin, M. Hayashi, and L. Thomas, Magnetic domain-wall racetrack memory, Science **320**, 190 (2008).

[19] D. Pinna, F. Abreu Araujo, J.-V. Kim, V. Cros, D. Querlioz, P. Bessiere, J. Droulez, and J. Grollier, Skyrmion gas manipulation for probabilistic computing, Phys. Rev. Appl. **9**, 064018 (2018).

[20] Y. Jibiki, M. Goto, E. Tamura, J. Cho, S. Miki, R. Ishikawa, H. Nomura, T. Srivastava, W. Lim, S. Auffret, C. Baraduc, H. Bea, and Y. Suzuki, Skyrmion Brownian circuit implemented in continuous ferromagnetic thin film, Appl. Phys. Lett. **117**, 082402 (2020).

[21] H. Orihara and Y. Ishibashi, A statistical theory of nucleation and growth in finite systems, J. Phys. Soc. Jpn. **61**, 1919 (1992).

[22] J. F. Scott, Device physics of ferroelectric memories, Ferroelectrics **183**, 51 (1996).

[23] W. J. Merz, Domain formation and domain wall motions in ferroelectric $BaTiO_3$ single crystals, Phys. Rev. **95**, 690 (1954).

[24] R. C. Miller and G. Weinreich, Mechanism for the sidewise motion of 180° domain walls in barium titanate, Phys. Rev. **117**, 1460 (1960).

[25] Y.-H. Shin, I. Grinberg, I.-W. Chen, and A. M. Rappe, Nucleation and growth mechanism of ferroelectric domain-wall motion, Nature (London) **449**, 881 (2007).

[26] T. Tybell, P. Paruch, T. Giamarchi, and J.-M. Triscone, Domain wall creep in epitaxial ferroelectric $Pb(Zr_{0.2}Ti_{0.8})O_3$ thin films, Phys. Rev. Lett. **89**, 097601 (2002).

[27] P. Paruch and J. Guyonnet, Nanoscale studies of ferroelectric domain walls as pinned elastic interfaces, C. R. Phys. **14**, 667 (2013).

[28] S. Liu, I. Grinberg, and A. M. Rappe, Exploration of the intrinsic inertial response of ferroelectric domain walls via molecular dynamics simulations, Appl. Phys. Lett. **103**, 232907 (2013).

[29] X. Li, T. Qiu, J. Zhang, E. Baldini, J. Lu, A. M. Rappe, and K. A. Nelson, Terahertz field induced ferroelectricity

in quantum paraelectric $SrTiO_3$, Science **364**, 1079 (2019).

[30] S. Prosandeev, S. Prokhorenko, Y. Nahas, J. Grollier, D. Talbayev, B. Dkhil, and L. Bellaiche, Ultrafast activation and tuning of topological textures in ferroelectric nanostructures, Adv. Electron. Mater. **8**, 2200808 (2022).

[31] S. Prosandeev, S. Prokhorenko, Y. Nahas, Y. Yang, C. Xu, J. Grollier, D. Talbayev, B. Dkhil, and L. Bellaiche, Designing polar textures with ultrafast neuromorphic features from atomistic simulations, Neuromorph. Comput. Eng. **3**, 012002 (2023).

[32] M. Zajac, T. Zhou, T. Yang, S. Das, Y. Cao, B. Guzelturk, V. Stoica, M. J. Cherukara, J. W. Freeland, V. Gopalan, R. Ramesh, L. W. Martin, L.-Q. Chen, M. V. Holt, S. O. Hruszkewycz, and H. Wen, Optical control of adaptive nanoscale domain networks, Adv. Mater. **36**, 2405294 (2024).

[33] L. Bastogne, F. Gómez-Ortiz, S. Anand, and P. Ghosez, Dynamical manipulation of polar topologies from acoustic phonon excitations, Nano Lett. **24**, 13783 (2024).

[34] W. Jiang, X. Zhang, G. Yu, W. Zhang, X. Wang, M. Benjamin Jungfleisch, J. E. Pearson, X. Cheng, O. Heinonen, K. L. Wang, Y. Zhou, A. Hoffmann, and S. G. E. te Velthuis, Direct observation of the skyrmion Hall effect, Nat. Phys. **13**, 162 (2017).

[35] V. T. Pham, N. Sisodia, I. D. Manici, J. Urrestarazu-Larrañaga, K. Bairagi, J. Pelloux-Prayer, R. Guedas, L. D. Buda-Prejbeanu, S. Auffret, A. Locatelli, T. O. Menteş, S. Pizzini, P. Kumar, A. Finco, V. Jacques, G. Gaudin, and O. Boulle, Fast current-induced skyrmion motion in synthetic antiferromagnets, Science **384**, 307 (2024).

[36] X. Gonze, B. Amadon, G. Antonius, F. Arnardi, L. Baguet, J.-M. Beuken, J. Bieder, F. Bottin, J. Bouchet, E. Bousquet *et al.*, The ABINIT project: Impact, environment and recent developments, Comput. Phys. Commun. **248**, 107042 (2020).

[37] D. R. Hamann, Optimized norm-conserving Vanderbilt pseudopotentials, Phys. Rev. B **88**, 085117 (2013).

[38] M. J. Van Setten, M. Giantomassi, E. Bousquet, M. J. Verstraete, D. R. Hamann, X. Gonze, and G.-M. Rignanese, The PSEUDODOJO: Training and grading a 85 element optimized norm-conserving pseudopotential table, Comput. Phys. Commun. **226**, 39 (2018).

[39] L. Bastogne and P. Ghosez, A second-principles open-source model to explore ferroelectric and topological textures in $PbTiO_3$ (unpublished).

[40] S. Duane, A. D. Kennedy, B. J. Pendleton, and D. Roweth, Hybrid Monte Carlo, Phys. Lett. B **195**, 216 (1987).

[41] M. Betancourt, A conceptual introduction to Hamiltonian Monte Carlo, arXiv:1701.02434.

[42] X. Gonze and C. Lee, Dynamical matrices, Born effective charges, dielectric permittivity tensors, and interatomic force constants from density-functional perturbation theory, Phys. Rev. B **55**, 10355 (1997).

[43] J. C. Wojdeł and J. Iniguez, Ferroelectric transitions at ferroelectric domain walls found from first principles, Phys. Rev. Lett. **112**, 247603 (2014).

[44] M. A. P. Gonçalves, C. Escorihuela-Sayalero, P. Garca-Fernández, J. Junquera, and J. Íñiguez, Theoretical guidelines to create and tune electric skyrmion bubbles, Sci. Adv. **5**, eaau7023 (2019).

[45] V. Stepkova, P. Marton, and J. Hlinka, Ising lines: Natural topological defects within ferroelectric bloch walls, Phys. Rev. B **92**, 094106 (2015).

[46] F. Gómez-Ortiz, L. Bastogne, S. Anand, M. Yu, X. He, and P. Ghosez, Switchable skyrmion-antiskyrmion tubes in rhombohedral $BaTiO_3$ and related materials, arXiv:2411.16395.

[47] C. Dai, Z. Hong, S. Das, Y.-L. Tang, L. W. Martin, R. Ramesh, and L.-Q. Chen, Strain effects on stability of topological ferroelectric polar configurations in $(PbTiO_3)_n/(SrTiO_3)_n$ superlattices, Appl. Phys. Lett. **123**, 052903 (2023).

[48] Z. Hong, A. R. Damodaran, F. Xue, S.-L. Hsu, J. Britson, A. K. Yadav, C. T. Nelson, J.-J. Wang, J. F. Scott, L. W. Martin, R. Ramesh, and L.-Q. Chen, Stability of polar vortex lattice in ferroelectric superlattices, Nano Lett. **17**, 2246 (2017).

[49] J. Íñiguez-González and H. Aramberri, Creating currents of electric bubbles, arXiv:2412.15074.

[50] L. Qin, Y. Huang, F. Xia, L. Wang, J. Ning, H. Chen, X. Wang, W. Zhang, Y. Peng, Q. Liu, and Z. Zhang, 5 nm nanogap electrodes and arrays by super-resolution laser lithography, Nano Lett. **20**, 4916 (2020).